

## Phase stability and transition of BaSi<sub>2</sub>-type disilicides and digermanides

Jian-Tao Wang,<sup>1,2,\*</sup> Changfeng Chen,<sup>2</sup> and Yoshiyuki Kawazoe<sup>3,4</sup>

<sup>1</sup>Beijing National Laboratory for Condensed Matter Physics, Institute of Physics, Chinese Academy of Sciences, Beijing 100190, China

<sup>2</sup>Department of Physics and High Pressure Science and Engineering Center, University of Nevada, Las Vegas, Nevada 89154, USA

<sup>3</sup>New Industry Creation Hatchery Center, Tohoku University, Sendai 980-8579, Japan

<sup>4</sup>Institute of Thermophysics, Siberian Branch of Russian Academy of Sciences, Novosibirsk 630090, Russia

(Received 20 October 2014; published 17 February 2015)

BaSi<sub>2</sub>-type disilicides and digermanides hold great promise for solar-cell applications, but their structural stability and phase transition mechanisms remain unresolved. Here we present *ab initio* calculations of pressure-induced structural phase transitions of BaSi<sub>2</sub>, BaGe<sub>2</sub>, and SrGe<sub>2</sub> and show that Si tetrahedra in orthorhombic BaSi<sub>2</sub> tend to convert to corrugated layers in the trigonal phase under high pressure with bond breaking along the *b* axis, and a three-dimensional Si net in the cubic phase is stabilized energetically at low pressure. The orthorhombic semiconductor-to-trigonal metal conversion is also preferred for SrGe<sub>2</sub> both energetically and kinetically. However, Ge tetrahedra in BaGe<sub>2</sub> tend to convert to a ThSi<sub>2</sub>-type tetragonal net with bond breaking around the *c* axis. The kinetic barriers are large for both the reaction ( $\sim 0.43$  eV under compression) and the counter-reaction ( $\sim 0.39$  eV under decompression) for BaSi<sub>2</sub>, which explains the stability of the trigonal and cubic phases at room temperature and the high-temperature requirement for the phase transitions.

DOI: [10.1103/PhysRevB.91.054107](https://doi.org/10.1103/PhysRevB.91.054107)

PACS number(s): 61.50.Ks, 62.50.-p, 64.70.kg

The BaSi<sub>2</sub>-type disilicides and digermanides BaSi<sub>2</sub>, SrSi<sub>2</sub>, BaGe<sub>2</sub>, and SrGe<sub>2</sub> are semiconductors with larger band gaps, 0.9–1.3 eV, and high optical absorption coefficients [1–4], which make them ideal candidates as silicon-based solar cell materials. Great interest in these materials has been reignited by the recent success in preparing well-crystalline *a*-axis-oriented BaSi<sub>2</sub> and Ba<sub>1-x</sub>Sr<sub>x</sub>Si<sub>2</sub> epitaxial films on Si(111) and Si(100) substrates [5–10]. It was demonstrated that the electronic band gap can reach the ideal value of approximately 1.4 eV by replacing half of the Ba atoms with isoelectric Sr atoms [5]. Meanwhile, there is a rich variety of pressure-induced structural phase transitions similar to those observed in Si and Ge [11]. Under ambient conditions, BaSi<sub>2</sub>, BaGe<sub>2</sub>, and SrGe<sub>2</sub> all adopt the BaSi<sub>2</sub>-type orthorhombic structure, but SrSi<sub>2</sub> has the SrSi<sub>2</sub>-type cubic structure [12–19]. Under high-pressure and high-temperature (HPHT) conditions, orthorhombic BaSi<sub>2</sub> transforms into SrSi<sub>2</sub>-type cubic and EuGe<sub>2</sub>-type trigonal structures [20–22], and the trigonal phase can exist under ambient conditions, showing a metallic and superconducting behavior [23]. On the other hand, orthorhombic BaGe<sub>2</sub> and SrGe<sub>2</sub> [17,24,25] transform into tetragonal and trigonal structures, respectively. Each phase of disilicides and digermanides is characterized by a unique three-connected Si or Ge configuration: isolated tetrahedra in the orthorhombic phase; two-dimensional, three-connected (2D3C) corrugated layers in the trigonal phase; and three-dimensional, three-connected (3D3C) nets in both cubic and tetragonal phases. As far as we know, a metallic phase formed under high pressure rarely exists at atmospheric pressure and room temperature. Past studies have explored the electronic, thermoelectric, and optical properties of these materials [26–28], but the more complicated and important atomistic mechanisms for the phase stability and pressure-induced phase transformations remain unresolved.

In this paper, we present a comprehensive study of the phase stability and transition of BaSi<sub>2</sub> compared with BaGe<sub>2</sub> and SrGe<sub>2</sub> over the wide pressure range of 0–10 GPa. We examine the energetics and kinetics that govern the phase stability and drive the structural conversion. In particular, we identify the pathways from the tetrahedral configurations in the orthorhombic phase toward the 2D3C corrugated layers in the trigonal phase and the 3D3C nets in the cubic phase with the Si-Si bond breaking and reconstruction parallel to the *b*[010] axis. Si tetrahedra in orthorhombic BaSi<sub>2</sub> convert to corrugated layers dynamically under high pressure, which further convert to 3D3C cubic nets under low pressure ( $< 7$  GPa) driven by energetics. Direct conversion from the orthorhombic (semiconductor) to the trigonal (metal) structure is also favored for SrGe<sub>2</sub> by both energetics and kinetics. Moreover, Ge tetrahedra in BaGe<sub>2</sub> tend to form a 3D3C tetragonal net structure with bond breaking and rebonding around the *c*[001] axis. Pressure plays a key role in enhancing the high-pressure phase stability, but it has little effect on the conversion barrier. The large counter-reaction barriers ( $\sim 0.39$  eV) are comparable to the compression process reaction barriers ( $\sim 0.43$  eV) for BaSi<sub>2</sub>, which explains the high stability of the HPHT metastable (cubic or trigonal) phases at room temperature and the requirement of high temperature for the phase transitions [20], in contrast to the low-kinetic-barrier, cold-compressed phase transitions in Si and Ge [11].

Our calculations are carried out using density functional theory as implemented in the Vienna *ab initio* simulation package (VASP) [29] with the spin-polarized generalized gradient approximation [30]. The all-electron projector augmented wave (PAW) method [31] was adopted, with  $4s^2 4p^6 5s^2$  for Sr,  $5s^2 5p^6 6s^2$  for Ba,  $3s^2 3p^2$  for Si, and  $3d^{10} 4s^2 4p^2$  for Ge treated as valence electrons. A plane-wave basis set with an energy cutoff of 500 eV was used. The phase conversion barrier was calculated using a generalized solid-state nudged elastic band method [32] with cell and atomic position optimization. Forces on the ions are calculated through the Hellmann-Feynman theorem,

\*wjt@aphy.iphy.ac.cn

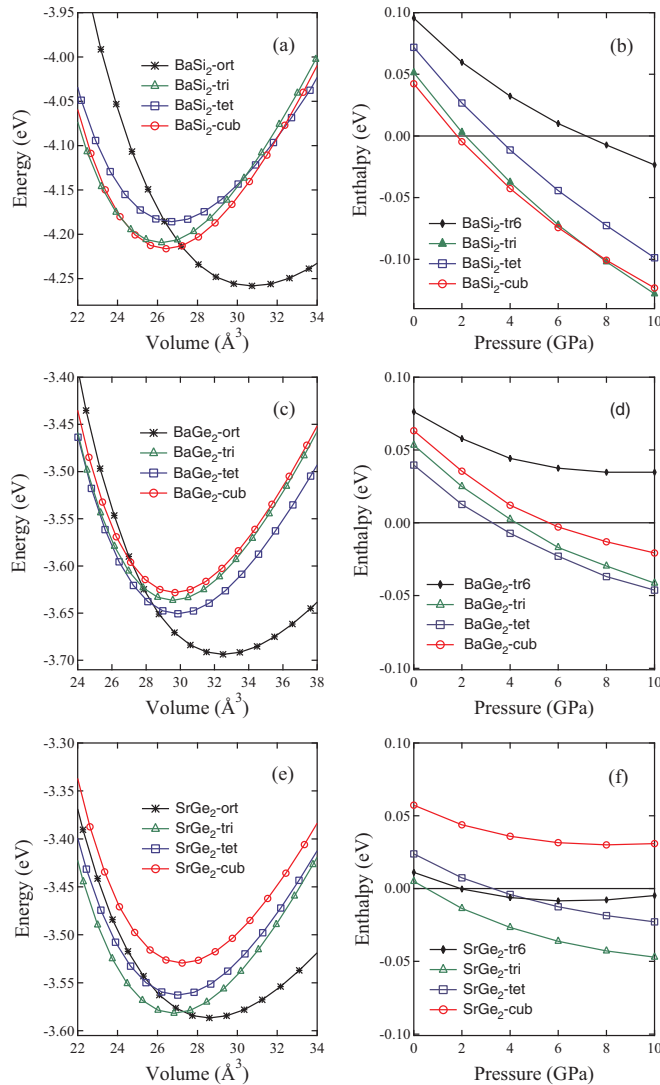


FIG. 1. (Color online) Energy versus volume per atom for BaSi<sub>2</sub> (a), BaGe<sub>2</sub> (c), and SrGe<sub>2</sub> (e). Enthalpy per atom versus pressure for BaSi<sub>2</sub> (b), BaGe<sub>2</sub> (d), and SrGe<sub>2</sub> (f), relative to that of a BaSi<sub>2</sub>-type orthorhombic structure. The BaSi<sub>2</sub>-type orthorhombic (ort), SrSi<sub>2</sub>-type cubic (cub),  $\alpha$ -ThSi<sub>2</sub>-type tetragonal (tet), and EuGe<sub>2</sub>-type trigonal (tri) phases are in  $D_{2h}^{16}$ - $Pnma$ ,  $O^6$ - $P4_332$ ,  $D_{4h}^{19}$ - $I4_1/amd$ , and  $D_{3d}^3$ - $P\bar{3}m1$  symmetry, respectively. The enthalpy of a CaSi<sub>2</sub>-type structure (*tr6* in  $R\bar{3}m$  symmetry) [22] is shown for comparison.

allowing a full geometry optimization. Convergence criteria employed for both the electronic and the ionic relaxation were set to  $10^{-6}$  eV and 0.02 eV/Å for energy and force, respectively.

We first discuss the energetic stability of silicides and germanides. The results show that the most favorable structures are orthorhombic, with the relatively large volumes of 30.78, 32.53, and 28.61 Å<sup>3</sup> per atom for BaSi<sub>2</sub>, BaGe<sub>2</sub>, and SrGe<sub>2</sub> [see Figs. 1(a), 1(c), and 1(e)], respectively. Meanwhile, the second stable phases have distinct cubic, tetragonal, or trigonal structures, with the relatively small volumes of 26.43, 29.86, and 26.83 Å<sup>3</sup> per atom. Upon compression, for BaSi<sub>2</sub> as shown in Fig. 1(b), the cubic structure becomes more stable than the

TABLE I. Calculated equilibrium lattice parameters  $a$ ,  $b$ , and  $c$  (in Å), volume (in Å<sup>3</sup> per atom), and bulk modulus ( $B_0$  in GPa) for BaSi<sub>2</sub>, BaGe<sub>2</sub>, and SrGe<sub>2</sub> in orthorhombic (ort), cubic (cub), tetragonal (tet), and trigonal (tri) symmetry at 0 GPa, compared to available experimental data. [17–19,22,24,25]

Phase	Method	$a$ (Å)	$b$ (Å)	$c$ (Å)	$V_0$ (Å <sup>3</sup> )	$B_0$ (GPa)
BaSi <sub>2</sub> -ort	Cal	9.224	6.827	11.716	30.78	28.23
	Exp [19,22]	8.942	6.733	11.555	28.99	27.94
BaSi <sub>2</sub> -tri	Cal	4.102	4.102	5.445	26.41	44.46
	Exp [19]	4.047	4.047	5.330	25.21	
BaSi <sub>2</sub> -cub	Cal	6.820	6.820	6.820	26.43	48.24
	Exp [19]	6.715	6.715	6.715	25.24	
BaSi <sub>2</sub> -tet	Cal	4.736	4.736	14.287	26.71	40.84
BaGe <sub>2</sub> -ort	Cal	9.471	6.942	11.861	32.53	25.14
	Exp [24]	9.078	6.829	11.653	30.10	
BaGe <sub>2</sub> -tri	Cal	4.344	4.344	5.435	29.59	38.60
BaGe <sub>2</sub> -cub	Cal	7.088	7.088	7.088	29.68	38.31
BaGe <sub>2</sub> -tet	Cal	4.882	4.882	15.031	29.86	35.64
	Exp [25]	4.769	4.769	14.737	27.93	
SrGe <sub>2</sub> -ort	Cal	9.058	6.674	11.351	28.61	29.12
	Exp [17]	8.739	6.567	11.215	26.82	
SrGe <sub>2</sub> -tri	Cal	4.204	4.204	5.256	26.83	41.50
	Exp [18]	4.104	4.104	5.165	25.11	
SrGe <sub>2</sub> -cub	Cal	6.887	6.887	6.887	27.23	41.62
SrGe <sub>2</sub> -tet	Cal	4.693	4.693	14.716	27.01	39.78

orthorhombic structure at 1.9 GPa, and the trigonal structure becomes more stable than the cubic structure above 7.2 GPa. The larger enthalpy change between the orthorhombic and the cubic phases shows a strong pressure dependence with a large volume change, while the small enthalpy change between the cubic and the trigonal phases has a corresponding small volume change (see Table I). On the other hand, for BaGe<sub>2</sub> and SrGe<sub>2</sub>, as shown in Figs. 1(d) and 1(f), no stable cubic phase exists up to 10 GPa. The tetragonal and trigonal structures become more stable than the orthorhombic structure above 3.2 and 0.52 GPa, respectively. The enthalpy of the CaSi<sub>2</sub>-type structure (*tr6* in  $R\bar{3}m$  symmetry) is also shown in Figs. 1(b), 1(d), and 1(f) for comparison [22], but it is clearly unfavorable for BaSi<sub>2</sub>, BaGe<sub>2</sub>, and SrGe<sub>2</sub> over the wide pressure range of 0–10 GPa.

It is worth noting that all of the Si and Ge sublattices satisfy the (8-N) rule, which requires a formal transfer of valence electrons from the divalent metal atoms to Si or Ge atoms [24], which then become isoelectronic with group V elements. One can regard BaSi<sub>2</sub> formally as Ba<sup>2+</sup>[Si<sup>-</sup>]<sub>2</sub>, and accordingly, Si<sub>4</sub> tetrahedra are preferred in the orthorhombic phase, which is similar to the structural arrangement in white phosphorus [33]. Since the orthorhombic phases have a high compressibility with a larger volume and a smaller bulk modulus (see Table I), the more densely packed cubic, trigonal, or tetragonal phases can be produced under pressure. Here the corrugated layers of Si in the trigonal phase are similar to the crystal structures adopted by black phosphorus at high pressures [34], and the cubic Si nets are congruent to the pressure-induced structure of cubic gauche nitrogen (cg-N) [35].

We next examine the kinetic process at the atomic scale using a generalized solid-state climbing image nudged

elastic band method [32] with cell and atomic position optimization under the wide pressure range of 0–8 GPa. According to the above results, there are three possible phase transformations from the BaSi<sub>2</sub>-type orthorhombic structure toward the SrSi<sub>2</sub>-type cubic, ThSi<sub>2</sub>-type tetragonal, and EuGe<sub>2</sub>-type trigonal phases under pressure. For transformation of the orthorhombic BaSi<sub>2</sub> to the cubic BaSi<sub>2</sub> phase [see Fig. 2(a)],  $b_{\text{ort}} = 6.827 \text{ \AA} \rightarrow a_{\text{cub}} = 6.820 \text{ \AA}$ ,  $c_{\text{ort}} = 11.716 \text{ \AA} \rightarrow \sqrt{2}a_{\text{cub}} = 9.645 \text{ \AA}$ , and  $a_{\text{ort}} = 9.224 \text{ \AA} \rightarrow \sqrt{2}a_{\text{cub}} = 9.645 \text{ \AA}$ , with about  $-18\%$  shortening in the  $c_{\text{ort}}$  direction and about  $+4.6\%$  elongation in the  $a_{\text{ort}}$  direction. Meanwhile, four Si<sub>4</sub> tetrahedra convert to four fourfold helices with bond breaking along the  $b[010]$  direction and rebonding with torsion angles of  $60^\circ$  between the helical chains to form the 3D3C cubic net [36]. Throughout this pathway, the intermediate structures are all in  $P2_1$  (No. 4) monoclinic symmetry, and the  $\angle\text{Si-Si-Si}$  bond angle changes from  $60^\circ$  in Si<sub>4</sub> tetrahedra to  $118^\circ$  in fourfold helices. As a result, one orthorhombic unit cell is converted into two cubic unit cells with four fourfold helices. For transformation of the orthorhombic BaSi<sub>2</sub> into the trigonal BaSi<sub>2</sub> phase [see Fig. 2(b)],  $b_{\text{ort}} = 6.827 \text{ \AA} \rightarrow \sqrt{3}a_{\text{tri}} = 7.105 \text{ \AA}$ ,  $a_{\text{ort}} = 9.224 \text{ \AA} \rightarrow 2a_{\text{tri}} = 8.204 \text{ \AA}$ , and  $c_{\text{ort}} = 11.716 \text{ \AA} \rightarrow 2c_{\text{tri}} = 10.890 \text{ \AA}$ , with about  $-7\%$  shortening in the  $c_{\text{ort}}$ ,  $-11\%$  shortening in the  $a_{\text{ort}}$ , and  $+4\%$  elongation in the  $b_{\text{ort}}$  direction. Along this pathway, four Si<sub>4</sub> tetrahedra convert to four distorted chains (parallel to the  $b[010]$  direction) with the bond breaking perpendicular to the  $c[001]$  axis, and then four chains rebond to each other to form corrugated Si layers with distorted six-membered rings. Throughout this pathway, the intermediate structures are all in  $P2_1/C$  (No. 14) monoclinic symmetry, and the  $\angle\text{Si-Si-Si}$  bond angle changes from  $60^\circ$  to  $111.6^\circ$ . As a result, one orthorhombic unit cell turns into four hexagonal cells. On the other hand, for transformation of the orthorhombic BaSi<sub>2</sub> into the tetragonal BaSi<sub>2</sub> phase [see Fig. 2(c)],  $b_{\text{ort}} = 6.827 \text{ \AA} \rightarrow \sqrt{2}a_{\text{tet}} = 6.698 \text{ \AA}$ ,  $a_{\text{ort}} = 9.224 \text{ \AA} \rightarrow \sqrt{2}a_{\text{tet}} = 6.698 \text{ \AA}$ , and  $c_{\text{ort}} = 11.716 \text{ \AA} \rightarrow c_{\text{tet}} = 14.287 \text{ \AA}$ , with about  $-27\%$  shortening in the  $a_{\text{ort}}$  direction and about  $+22\%$  elongation in the  $c_{\text{ort}}$  direction. Along the pathway, four Si<sub>4</sub> tetrahedra convert to four flat Si<sub>4</sub> groups with bond breaking around the  $c[001]$  axis, and then the four flat Si<sub>4</sub> groups rebond to each other to form a 3D3C tetragonal net [see Fig. 2(c)]. Throughout this pathway, the intermediate structures are all in  $P2_12_12_1$  (No. 19) orthorhombic symmetry, and the  $\angle\text{Si-Si-Si}$  bond angle changes from  $60^\circ$  to  $120^\circ$ . As a result, one orthorhombic unit cell is converted into two tetragonal unit cells.

Figure 3(a) shows the enthalpy along the pathways starting from orthorhombic BaSi<sub>2</sub> toward the formation of the cubic, tetragonal, and trigonal BaSi<sub>2</sub> phases at 4 GPa. The enthalpy increases initially due to the bond twisting and breaking of the Si<sub>4</sub> tetrahedra in the orthorhombic phase, and then it decreases with the relinking of Si-Si bonds. The conversion barriers are estimated to be 0.424 eV for orthorhombic  $\rightarrow$  cubic, 0.430 eV for orthorhombic  $\rightarrow$  trigonal, and 0.434 eV for orthorhombic  $\rightarrow$  tetragonal. These results suggest a strongly competitive nature to form the cubic, trigonal, and tetragonal structures. A similar competitive nature is also found in the hypothetical conversion of orthorhombic SrSi<sub>2</sub> [37]. Among these reactions, however, the pathway

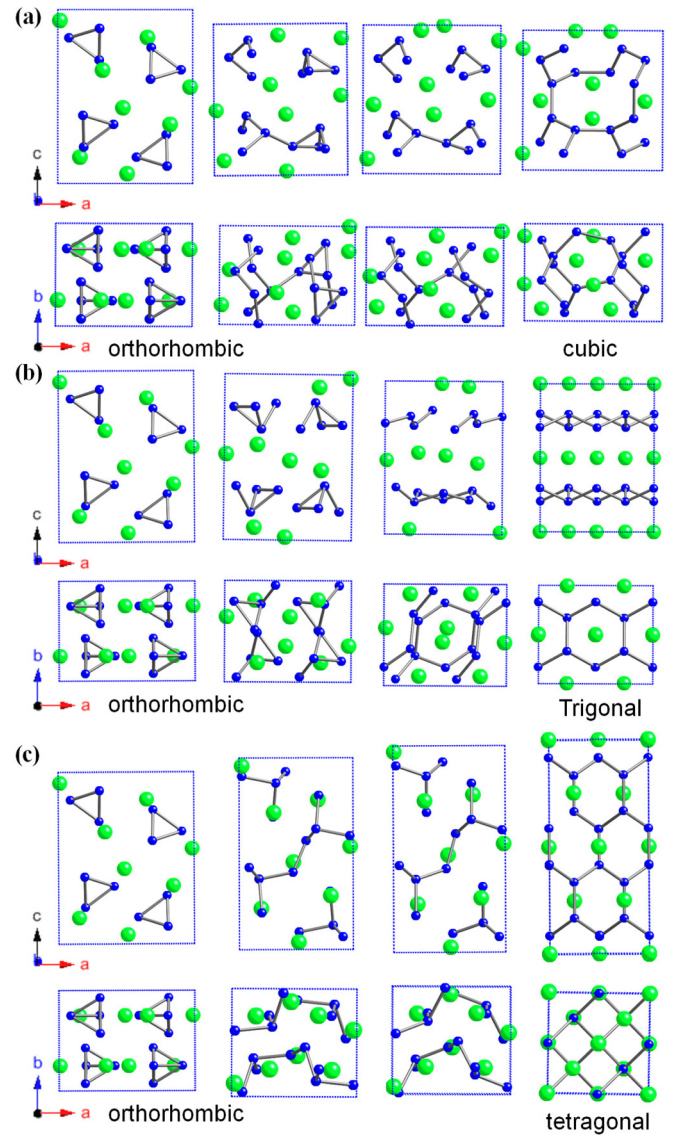


FIG. 2. (Color online) Top and side views of the structures along the pathways to form cubic, trigonal, and tetragonal BaSi<sub>2</sub> starting from the orthorhombic phase at 4 GPa. (a) Conversion process orthorhombic  $\rightarrow$  cubic with bond breaking along the  $b[010]$  direction. The intermediate structures along the pathway are in  $P2_1$  (No. 4) monoclinic symmetry. (b) Conversion process orthorhombic  $\rightarrow$  trigonal with shortening in the  $a_{\text{ort}}$  and  $c_{\text{ort}}$  directions and elongation in the  $b_{\text{ort}}$  direction. The intermediate structures along the pathway are in  $P2_1/C$  (No. 14) monoclinic symmetry. (c) Conversion process orthorhombic  $\rightarrow$  tetragonal with shortening in the  $a_{\text{ort}}$  direction and elongation in the  $c_{\text{ort}}$  direction. The intermediate structures along the pathway are in  $P2_12_12_1$  (No. 19) orthorhombic symmetry. Small (blue) and large (green) circles denote Si and Ba atoms, respectively.

toward the trigonal phase has the lowest enthalpy up to step 8 as shown in Fig. 3(a). Thus the orthorhombic-to-trigonal transition is more favored dynamically than the orthorhombic-to-cubic transition. Experimentally, a two-stage reaction process of orthorhombic  $\rightarrow$  trigonal  $\rightarrow$  cubic is shown at 5.2 GPa up to 1133 K [20]. To clarify this point,

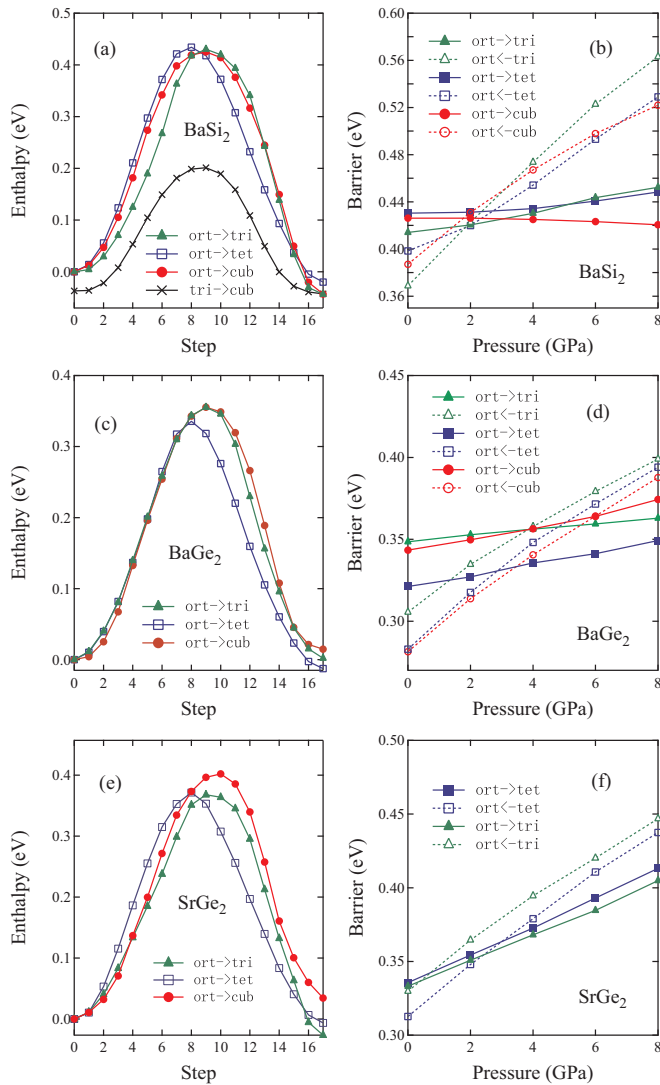


FIG. 3. (Color online) (a), (c), (e) Enthalpy versus transformation pathways orthorhombic  $\rightarrow$  cubic, orthorhombic  $\rightarrow$  trigonal, and orthorhombic  $\rightarrow$  tetragonal at 4 GPa for BaSi<sub>2</sub>, BaGe<sub>2</sub>, and SrGe<sub>2</sub>, respectively. (b), (d), (f) Enthalpy barriers versus pressure for orthorhombic  $\rightarrow$  cubic, orthorhombic  $\rightarrow$  tetragonal, and orthorhombic  $\rightarrow$  trigonal, respectively.

we have also examined the second-stage trigonal-to-cubic conversion process [37], and the corresponding enthalpy is plotted in Fig. 3(a). The conversion barrier is estimated as 0.24 eV at 4 GPa, which is lower than the 0.43 eV for the first-stage orthorhombic-to-trigonal conversion. Consequently, cubic BaSi<sub>2</sub> can be easily synthesized by a two-stage reaction process.

We plot in Fig. 3(b) the enthalpy barriers versus pressure. With increasing pressure from 0 to 8 GPa, the barriers undergo only small changes: from 0.429 to 0.421 eV for orthorhombic  $\rightarrow$  cubic, from 0.411 to 0.452 eV for orthorhombic  $\rightarrow$  trigonal, and from 0.430 to 0.448 eV for orthorhombic  $\rightarrow$  tetragonal. These results show that pressure has little effect on the conversion barrier, which means that these phase conversions require high temperatures to overcome the large energy barriers. This

is similar to the situation of phase conversion of graphite to diamond [38].

Experimentally, it has been reported that both the cubic and the trigonal phases of BaSi<sub>2</sub> can be quenched to the ambient conditions [20]. To clarify this point, the counter-reaction barriers are also plotted in Fig. 3(b). With decreasing pressure from 8 to 0 GPa, the barriers decrease from 0.522 to 0.387 eV for cubic  $\rightarrow$  orthorhombic, from 0.563 to 0.369 eV for trigonal  $\rightarrow$  orthorhombic, and from 0.529 to 0.398 eV for tetragonal  $\rightarrow$  orthorhombic. These results suggest that pressure has a considerable effect on lowering the kinetic barrier upon decompression. However, the counter-reaction barriers remain at high values ( $\sim 0.39$  eV at 0 GPa) that are comparable to the barriers encountered during the compression process ( $\sim 0.43$  eV). As a result, the cubic and trigonal phases can be stabilized under ambient conditions due to a combination of the large counter-reaction barriers ( $\sim 0.39$  eV) and small energy differences ( $\sim 0.05$  eV per atom) relative to the BaSi<sub>2</sub>-type orthorhombic structure [see Fig. 1(b)].

For BaGe<sub>2</sub>, as shown in Figs. 3(c) and 3(d), the orthorhombic  $\rightarrow$  tetragonal conversion is clearly favorable both kinetically and energetically. On the other hand, for SrGe<sub>2</sub> compound, the cubic structure is unfavorable in enthalpy as shown in Fig. 1(f) over the wide pressure range of 0–10 GPa. There is a strong competing conversion pathway under pressure to form the trigonal or tetragonal structure [see Figs. 3(e) and 3(f)]; however, the orthorhombic  $\rightarrow$  trigonal conversion is more favorable dynamically, similar to the case of BaSi<sub>2</sub> discussed above.

In summary, our *ab initio* calculations have revealed the phase stability and transformation mechanisms for several BaSi<sub>2</sub>-type semiconductors. The results show that the tetrahedra in orthorhombic BaSi<sub>2</sub> and SrGe<sub>2</sub> tend to convert to corrugated layers dynamically under high pressure with bond breaking along the  $b[010]$  axis, and the Si-corrugated layers in trigonal BaSi<sub>2</sub> can further convert to cubic Si nets under low pressure driven by energetics. Moreover, Ge tetrahedra in BaGe<sub>2</sub> tend to form a tetragonal-net structure with bond breaking around the  $c[001]$  axis. The large counter-reaction barriers ( $\sim 0.39$  eV) are comparable to those for the compression process reaction barriers ( $\sim 0.43$  eV) for BaSi<sub>2</sub>, which explains the high stability of the metastable phases under ambient conditions. Our results provide a comprehensive understanding of the experimental findings by unveiling the underlying energetic and kinetic mechanisms, which may shed light on other disilicides and digermanides.

We are thankful to the crew of the Center for Computational Materials Science at IMR, Tohoku University, for their support at the SR16000 supercomputing facilities. This study was supported by the NSFC (Grant No. 11274356) and the Strategic Priority Research Program of the CAS (Grant No. XDB07000000). C.F.C. acknowledges support by DOE under Cooperative Agreement No. DE-NA0001982. Y.K. acknowledges support by the CREST project, headed by Professor M. Kotani, and Russian Megagrant Project No. 14.B25.31.0030.

- [1] T. Nakamura, T. Suemasu, K. Takakura, F. Hasegawa, A. Wakahara, and M. Imai, *Appl. Phys. Lett.* **81**, 1032 (2002).
- [2] S. Kishino, T. Imai, T. Iida, Y. Nakaishi, M. Shinada, Y. Takanashi, and N. Hamada, *J. Alloys Compd.* **428**, 22 (2007).
- [3] Y. Matsumoto, D. Tsukada, R. Sasaki, M. Takeishi, and T. Suemasu, *Appl. Phys. Express* **2**, 021101 (2009).
- [4] M. Imai, *Phys. Status Solidi C* **10**, 1728 (2013).
- [5] T. Suemasu, K. Morita, and M. Kobayashi, *J. Cryst. Growth* **301–302**, 680 (2007).
- [6] M. Kobayashi, Y. Matsumoto, Y. Ichikawa, D. Tsukada, and T. Suemasu, *Appl. Phys. Express* **1**, 051403 (2008).
- [7] M. A. Khan, T. Saito, K. Nakamura, M. Baba, W. Du, K. Toh, K. Toko, and T. Suemasu, *Thin Solid Films* **522**, 95 (2012).
- [8] W. J. Du, M. Suzuno, M. Ajmal Khan, K. Toh, M. Baba, K. Nakamura, K. Toko, N. Usami, and T. Suemasu, *Appl. Phys. Lett.* **100**, 152114 (2012).
- [9] M. Ajmal Khan, K. O. Hara, W. Du, M. Baba, K. Nakamura, M. Suzuno, K. Toko, N. Usami, and T. Suemasu, *Appl. Phys. Lett.* **102**, 112107 (2013).
- [10] S. Koike, K. Toh, M. Baba, K. Toko, K. O. Hara, N. Usami, N. Saito, N. Yoshizawa, and T. Suemasu, *J. Crystal Growth* **378**, 198 (2013).
- [11] J. T. Wang, C. F. Chen, H. Mizuseki, and Y. Kawazoe, *Phys. Rev. Lett.* **110**, 165503 (2013).
- [12] H. K. Janzon, H. Schäfer, and A. Weiss, *Z. Anorg. Allg. Chem.* **372**, 87 (1970).
- [13] H. Schäfer, K. H. Janzon, and A. Weiss, *Angew. Chem. Int. Ed. Engl.* **2**, 393 (1963).
- [14] J. Evers, G. Oehlinger, and A. Weiss, *Angew. Chem. Int. Ed. Engl.* **17**, 538 (1978).
- [15] J. Evers, G. Oehlinger, and A. Weiss, *Angew. Chem. Int. Ed. Engl.* **16**, 659 (1977).
- [16] M. Pani and A. Palenzona, *J. Alloys Compd.* **462**, L9 (2008).
- [17] A. Palenzona and M. Pani, *J. Alloys Compd.* **402**, 136 (2005).
- [18] J. Evers, G. Oehlinger, and A. Weiss, *Z. Naturforsch. B* **32**, 1352 (1977).
- [19] J. Evers, *J. Solid State Chem.* **32**, 77 (1980).
- [20] M. Imai, T. Hirano, T. Kikegawa, and O. Shimomura, *Phys. Rev. B* **55**, 132 (1997); **58**, 11922 (1999).
- [21] J. Evers, *J. Solid State Chem.* **24**, 199 (1978); *J. Phys. Chem. Solid* **40**, 951 (1979).
- [22] M. Imai and T. Kikegawa, *Chem. Mater.* **15**, 2543 (2003).
- [23] M. Imai and T. Hirano, *J. Alloys Compd.* **224**, 111 (1995).
- [24] J. T. Vaughan, G. J. Miller, S. Gravelle, E. A. Leon-Escamilla, and J. D. Corbett, *J. Solid State Chem.* **133**, 501 (1997).
- [25] J. Evers, G. Oehlinger, and A. Weiss, *Z. Naturforsch. B* **35**, 397 (1980).
- [26] K. Hashimoto, K. Kurosaki, Y. Imamura, H. Muta, and S. Yamanaka, *J. Appl. Phys.* **102**, 063703 (2007).
- [27] D. B. Migas, V. L. Shaposhnikov, and V. E. Borisenko, *Phys. Status Solidi* **244**, 2611 (2007).
- [28] M. Kumar, N. Umezawa, and M. Imai, *J. Appl. Phys.* **115**, 203718 (2014).
- [29] G. Kresse and J. Furthmüller, *Phys. Rev. B* **54**, 11169 (1996); G. Kresse and J. Hafner, *ibid.* **47**, 558 (1993).
- [30] Y. K. Zhang and W. T. Yang, *Phys. Rev. Lett.* **80**, 890 (1998).
- [31] P. E. Blöchl, *Phys. Rev. B* **50**, 17953 (1994); G. Kresse and D. Joubert, *ibid.* **59**, 1758 (1999).
- [32] J. T. Wang, C. F. Chen, and Y. Kawazoe, *Phys. Rev. Lett.* **106**, 075501 (2011).
- [33] A. Simon, H. Borrmann, and H. Craubner, *Phosphorus Sulfur Related Elements* **30**, 507 (1987); H. Okudera, R. E. Dinnebier, and A. Simon, *Z. Kristallogr.* **220**, 259 (2005).
- [34] J. C. Jamieson, *Science* **139**, 1291 (1963).
- [35] M. I. Eremets, A. G. Gavriliuk, I. A. Trojan, D. A. Dzivenko, and R. Boehler, *Nature Mater.* **3**, 558 (2004).
- [36] J. T. Wang, C. F. Chen, and Y. Kawazoe, *Sci. Rep.* **3**, 3077 (2013).
- [37] See Supplemental Material at <http://link.aps.org/supplemental/10.1103/PhysRevB.91.054107> for the phase stability of hypothetical orthorhombic SrSi<sub>2</sub> (Fig. S1) and the conversion pathway between trigonal and cubic BaSi<sub>2</sub> (Fig. S2).
- [38] J. T. Wang, C. F. Chen, and Y. Kawazoe, *Phys. Rev. B* **84**, 012102 (2011).